ACS APPLIED MATERIALS & INTERFACES

Research Article

www.acsami.org

Highly Hydrophilic Thin-Film Composite Forward Osmosis Membranes Functionalized with Surface-Tailored Nanoparticles

Alberto Tiraferri,[†] Yan Kang,[‡] Emmanuel P. Giannelis,[‡] and Menachem Elimelech*[,†]

[†]Department of Chemical and Environmental Engineering, Yale University, New Haven, Connecticut 06520-8286, United States

[‡]Department of Materials Science and Engineering, Cornell University, Ithaca, New York 14853, United States

Supporting Information

ABSTRACT: Thin-film composite polyamide membranes are state-of-the-art materials for membrane-based water purification and desalination processes, which require both high rejection of contaminants and high water permeabilities. However, these membranes are prone to fouling when processing natural waters and wastewaters, because of the inherent surface physicochemical properties of polyamides. The present work demonstrates the fabrication of forward osmosis polyamide membranes with optimized surface properties via facile and scalable functionalization with fine-tuned nanoparticles. Silica nanoparticles are coated with superhydrophilic ligands possessing functional groups that impart stability to the nanoparticles and bind irreversibly to the native carboxyl moieties on the membrane selective layer. The tightly tethered layer of nanoparticles tailors the surface chemistry of the novel composite membrane without altering the morphology or water/solute permeabilities of the membrane selective layer. Surface characterization and interfacial energy analysis confirm that highly hydrophilic and wettable membrane surfaces are successfully attained. Lower intermolecular adhesion forces are measured between the new membrane materials and model organic foulants, indicating the presence of a bound hydration layer at the polyamide membrane surface that creates a barrier for foulant adhesion.

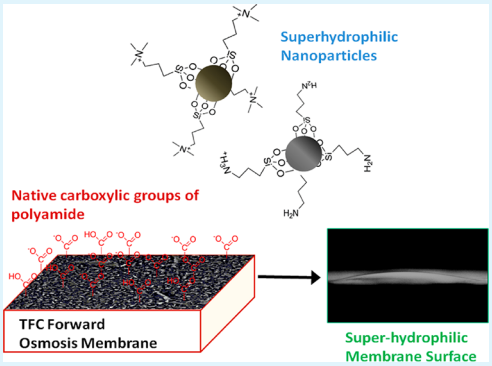

KEYWORDS: *thin-film composite membranes, forward osmosis, superhydrophilic, membrane functionalization, nanocomposite membranes, fouling, antifouling*

INTRODUCTION

Membrane-based technologies for desalination and wastewater reuse have the potential to sustainably increase the supply of potable and agricultural water.[1,2] Forward osmosis, which is a membrane-based separation process, is particularly attractive, because it can reduce the energy of separation.[3] Polyamide thin-film composite membranes are at the core of this technology,[1,4] because of their superior selectivity and water permeability.[4,5] However, polyamide membranes have relatively high fouling propensity, because of their inherent surface physicochemical properties.[6,7] Further development and implementation of processes utilizing polyamide membranes require significant improvement in their fouling resistance. The rational optimization of polyamide surface properties is a critical step in this endeavor.

Significant efforts have been made in membrane surface modification via post-fabrication procedures.[4,8,9] Recently, the use of nanomaterials has shown the potential as a novel strategy to tailor membrane surface characteristics.[10−12] Nanoparticles can be fine-tuned in terms of size, shape, and surface chemistry to achieve desired characteristics. Well-designed nanoparticles can have strong interactions with the membrane surface to ensure irreversible functionalization and retain the targeted property during operation. The effective combination of such materials with polymeric membranes would consist of non-depleting and scalable surface functionalizations that do not affect other crucial transport parameters of the membrane.

Recent studies have made use of antimicrobial nanoparticles with the goal to impart biocidal properties to polyamide membrane and control their biofouling.[11,12] These studies have suggested ways to permanently tether nanoparticles by exploiting the native functional groups of polyamide. In addition, it was shown that controlling the surface density and uniform distribution of the nanoparticle coating is especially important to concentrate the nanoparticle activity at the membrane surface.[12]

Inactivation of micro-organisms that attach to the membrane would delay the onset of biofilm formation.[13−15] However, the primary attachment mechanism of micro-organisms involves the secretion of protein-based adhesives.[16−18] In addition, many other organic molecules are present in feedstreams and contribute significantly to the decrease in process performance due to fouling. Therefore, the development of surface functionalizations that decrease the adhesion or increase the release of adsorbed organic molecules is of paramount importance.[1,17]

Received: August 2, 2012
Accepted: September 4, 2012
Published: September 4, 2012

   dx.doi.org/10.1021/am301532g | *ACS Appl. Mater. Interfaces* 2012, 4, 5044−5053

Scheme 1. Schematic of the Functionalized Nanoparticles and the Protocol Used To Functionalize the Thin-Film Composite Polyamide Forward Osmosis Membranes Used in This Study[a]

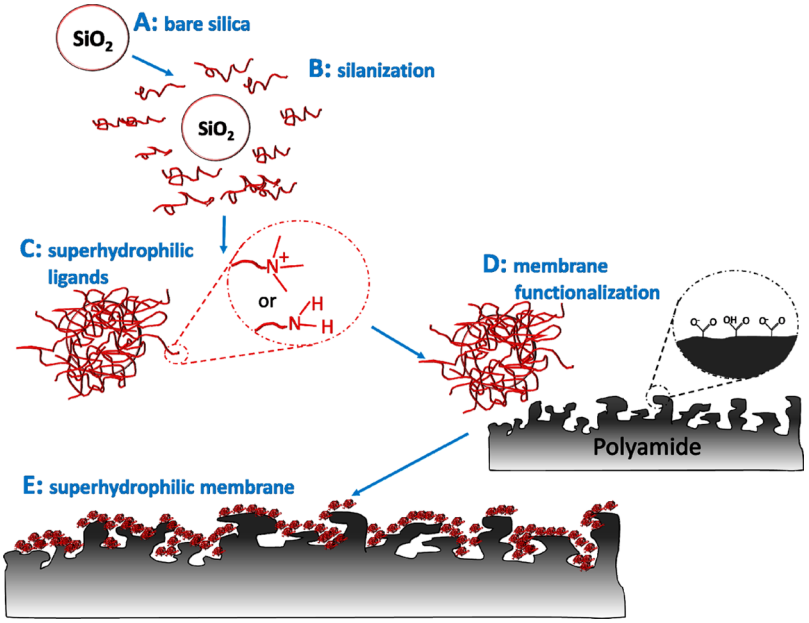

[a]Polyamide membranes possess native carboxylic groups at their surfaces that can be exploited as binding sites for functionalization with tailored nanoparticles. Two different ligands were used to tailor the surface of the nanoparticles, rendering them highly hydrophilic and optimizing their interaction with the membrane surface.

Wettability and hydrophilicity of the membrane material play a crucial role in controlling fouling resistance and release of adsorbed foulants, because these parameters are directly related to the material surface tension.[1,17,19] Specifically, by increasing the number of hydrogen bonding sites at the surface, the interfacial acid−base forces are maximized, thereby allowing the formation of an interfacial layer of tightly bonded water molecules that are highly oriented and have slow dynamics. Because the displacement of water molecules involves work that increases the free energy of the system, this hydration layer provides a repulsive barrier against the adsorption of foulants.[20] Studies have shown that increasing the membrane hydrophilicity can hinder fouling by micro-organisms,[21] proteins,[22−24] lipopolysaccharides,[23] inorganic colloids,[25] alginate,[26] and natural organic matter.[26]

The present study demonstrates the fabrication of highly hydrophilic thin-film composite polyamide forward osmosis membranes by surface functionalization with tailored nanoparticles. The proposed surface functionalization procedure is remarkably simple and effective, and follows the steps illustrated in Scheme 1. Silica nanoparticles (Step A) are surface-coated with superhydrophilic cationic ligands (Step B) to create a stable nanoparticle suspension. The ligands are terminated with either quaternary ammonium or amine functional groups (Step C), to stabilize the nanoparticles and to provide anchor sites for tethering the nanoparticles to the membranes. A dip-coating protocol is performed, during which the nanoparticles strongly bind to the native carboxyls of hand-cast polyamide forward osmosis membranes (Step D). The newly fabricated surfaces (Step E) are extensively characterized and their physicochemical properties, as well as their interfacial energies, are investigated. The new hydrophilic membranes have the potential to significantly improve membrane performance by reducing and delaying fouling.

MATERIALS AND METHODS

Fabrication of the Membranes and Characterization of Their Transport Properties. Thin-film composite (TFC) forward osmosis membranes were prepared by interfacial polymerization of polyamide onto hand-cast support membranes. The support membranes were fabricated by nonsolvent (water)-induced phase separation of a solution of 9 wt % polysulfone (PSf, M_n = 22 000 Da) dissolved in *N*,*N*-dimethylformamide (DMF, anhydrous, 99.8%), following the procedure outlined in our previous publication.[27] The polyamide active layer was then formed on top of the PSf support membranes via reaction between 1,3-phenylenediamine (MPD, >99%) and 1,3,5-benzenetricarbonyl trichloride (TMC, 98%) dissolved in Isopar-G (Univar, Redmond, WA), as described in our previous publication.[12]

The transport properties of the control and functionalized forward-osmosis membranes were tested using a cross-flow membrane filtration system in forward-osmosis and pressure retarded osmosis configurations.[28,29] These measurements allowed for the determination of the pure water permeability of the membrane active layer (A), the salt (NaCl) permeability of the membrane active layer (B), and the structural parameter of the membrane support layer (S), as 2.46 ± 1.19 L m^{-2} h^{-1} bar^{-1}, 1.70 ± 1.18 L m^{-2} h^{-1}, and 537 ± 182 μm, respectively (see Table S4 in the Supporting Information). Details of the characterization protocol can be found elsewhere.[30]

Fabrication and Characterization of the Superhydrophilic Nanoparticles. Superhydrophilic nanoparticles were fabricated by surface functionalization of silica nanoparticles (Ludox HS-30, 30%, Sigma−Aldrich) with two different ligands (Scheme 1, steps A−B−C). In the first instance, 6 g of silica nanoparticles were dispersed in 30 mL of deionized (DI) water and the suspension was sonicated for 30 min. The obtained dispersion was vigorously stirred with freshly prepared silane solution containing 2.1 g of (3-aminopropyl)trimethoxysilane ($-NH_3^+/NH_2$, 97%, Sigma−Aldrich 281778) dissolved in 24 mL of water. For the second functionalization, 6 g of silica nanoparticles were suspended in 54 mL of DI water and sonicated for 30 min. Then, 6.4 g of *N*-trimethoxysilylpropyl-*N*,*N*,*N*-trimethylammonium chloride ($-N-(CH_3)_3^+$, 50 wt %, Gelest SIT8415.0) were added to the dispersion under vigorous stirring. Both procedures were followed by pH adjustment to ∼5 and a heating step at 60 °C for 18 h. Finally, the

dx.doi.org/10.1021/am301532g | ACS Appl. Mater. Interfaces 2012, 4, 5044−5053

suspensions were dialyzed in DI water using SnakeSkin tubing (7k MWCO, Pierce) for 48 h.

Dynamic light scattering (DLS) experiments were performed to determine the effective hydrodynamic diameters of the functionalized nanoparticles using a multi-detector light scattering unit (ALV-5000, Langen, Germany), following the procedure outlined in our previous publication.[31] The electrophoretic mobility of the particles was determined by a Zetasizer Nano-Z (Malvern Instruments, Worcestershire, U.K.) in DI water at three different pH values of 5, 6, and 7. For thermogravimetric analysis (TGA) (Exstar TG/DTA 6200, Seiko Instruments, Inc., Torrance, CA), the nanoparticle solution was freeze-dried and TGA was performed from 40 °C to 600 °C at a heating rate of 20 °C/min. Transmission electron microscopy (TEM) micrographs of the nanoparticles were acquired using a Tecnai T12 apparatus operating at 120 keV (FEI, Eindhoven, The Netherlands).

Membrane Functionalization and Characterization. The density of carboxyl functional groups at the surface of polyamide membranes was evaluated by binding and elution of Toluidine Blue O dye (TBO), as described in our recent publication.[32] Carboxyl moieties were exploited to irreversibly bind the functionalized silica nanoparticles to the membranes, following a simple dip coating protocol (Scheme 1, steps D–E). Briefly, the polyamide membranes were immersed into the nanoparticle suspension for 16 h at room temperature (23 °C), with only the membrane active layer side being accessible for contact with the suspension. The pH of the suspensions was adjusted to between 6.4 and 7.4 before the dip-coating step. In the case of membrane functionalization with nanoparticles coated with amine-terminated ligands, the tethering procedure was preceded by contact of the polyamide layer with a solution of ∼2 mM *N*-(3-dimethylaminopropyl)-*N*′-ethylcarbodiimide hydrochloride (EDC, 98%), and ∼5 mM *N*-hydroxysuccinimide (NHS, 98%) for 15 min. The polyamide surface treatment with EDC and NHS converts the native carboxylate groups of the polyamide surface into intermediate amine-reactive esters[33] for crosslinking with the amine functional groups at the nanoparticle surface.

The elemental composition of the membrane surface was analyzed by X-ray photoelectron spectroscopy (XPS, SSX-100 UHV, Surface Science Instruments). The sample was irradiated with a beam of monochromatic Al Kα X-rays with energy of 1.486 keV. Attenuated total reflectance-infrared spectroscopy (ATR-IR, ThermoScientific Nicolet 6700) was performed using a germanium crystal on desiccator-dried samples. Membrane surface morphology was investigated by scanning electron microscopy (SEM, LEO 1550 FESEM). Before imaging, membranes were sputter-coated with a layer of carbon (BTT-IV, Denton Vacuum, LLC, Moorestown, NJ). Membrane surface roughness was analyzed using a Multimode AFM (Veeco Metrology Group, Santa Barbara, CA) in tapping mode. Symmetric silicon probes with 30-nm-thick back side aluminum coating were employed (Tap300A, Bruker Nano, Inc., Camarillo, CA). The probe had a spring constant of 40 N/m, resonance frequency of 300 kHz, tip radius of 8 ± 4 nm, and cantilever length of 125 ± 10 μm. Air-dried membranes were scanned in air at 12 randomly selected scan positions.

Surface wettability was evaluated from contact angle measurements of DI water using the sessile drop method (VCA Video Contact Angle System, AST Products, Billerica, MA). The system is equipped with software to determine the left and right contact angles (VCA Optima XE). To account for variations between different measurements on the same surface, at least 4 desiccator-dried samples from separately cast and functionalized membranes were tested on a minimum of six random locations, and the data were averaged. The relative wettability of the membranes was evaluated by calculating the membrane–liquid interfacial free energy as $-\Delta G_{ML} = \gamma_L(1 + (\cos\theta)/r)$, where θ is the average contact angle and γ_L is the pure water surface tension (72.8 mJ/m^2 at 25 °C), and r is the roughness area ratio (i.e., the ratio of actual surface area for a rough surface to the planar area, $r = 1 + SAD$, with SAD being the surface area difference parameter).[34,35] Contact angles of DI water were also used as a proxy to confirm the irreversibility of the nanoparticle–membrane bonds with functionalized membrane surfaces, after these were subjected to chemical or physical stress. Chemical stress was applied by contacting the functionalized surfaces for 15 min with a pH 2 solution (HCl), a pH 12 solution (NaOH), or a 0.6 M NaCl solution approximating the ionic strength of typical seawater, followed by a thorough rinse with DI water. Physical stress was exerted by immersing the membranes in a sonicating water bath (Fisher Scientific F60) for 7 min. XPS spectra and SEM images were also re-evaluated after each of these steps to confirm the presence and extent of particle functionalization and assess the irreversibility of the functionalization.

Additional measurements of contact angles of glycerol (≥99%) and diiodomethane (≥99%) were used to calculate the Lifshitz–van der Waals (γ^{LW}), electron donor (γ^-), and electron acceptor (γ^+) components of the membrane surface tension before and after functionalization.[36−38] In these calculations, the excess surface area due to roughness is taken into account by incorporation of the roughness area ratio (r), which was defined earlier. The total surface energy of the membrane surfaces is defined as the sum of the surface tension due to Lifshitz–van der Waals and Lewis acid-base components:

$$\gamma^{TOT} = \gamma^{LW} + \gamma^{AB}$$

where $\gamma^{AB} = 2(\gamma^+\gamma^-)^{1/2}$.[36,37] From the membrane and the water components of the surface tension, it is possible to calculate the total interfacial free energy of cohesion of membrane interfaces immersed in water, $\Delta G_{MLM}(TOT)$, which is often termed "hydrophilicity".[36−38] A higher value of the free energy is obtained if the membrane is noncohesive, or more hydrophilic, when immersed in water.

The zeta potential of the membrane surface before and after functionalization was measured in an asymmetric clamping cell using a streaming potential analyzer (EKA, Brookhaven Instruments, Holtsville, NY). Measurements were performed while alternating flow direction of a 1 mM KCl solution, and by varying the pH of the solution by adding appropriate amounts of HCl or KOH. Four separately cast and functionalized membranes were evaluated. A detailed experimental procedure and the method used to calculate the zeta potential from the measured streaming potential are given elsewhere.[39]

AFM Interaction Forces. Atomic force microscopy (AFM) was used to measure the adhesive force between representative foulants in the bulk solution and the membrane by adapting the procedures described by Li and Elimelech.[40] The force measurements were performed in a fluid cell utilizing a particle probe, modified from a commercialized SiN AFM probe (Veeco Metrology Group, Santa Barbara, CA). A carboxylate modified latex (CML) particle (Interfacial Dynamics Corp., Portland, OR) with a diameter of 4.0 μm was attached to the tipless SiN cantilever using Norland Optical adhesive (Norland Products, Inc., Cranbury, NJ). The particle probe was cured under UV light for 30 min. The CML-modified probe was immersed in a 2000 mg/L model organic foulant solution, namely alginate or bovine serum albumin (BSA), for at least 16 h at 4 °C, to prevent organic degradation. The AFM adhesion force measurements were performed in a fluid cell. The ionic composition of the test solutions injected into the fluid cell was representative of a typical wastewater effluent (0.45 mM KH_2PO_4, 9.20 mM NaCl, 0.61 mM $MgSO_4$, 0.5 $NaHCO_3$, 0.5 mM $CaCl_2$, and 0.935 mM NH_4Cl).[13] The pH of the test solution was adjusted to 7.4 prior to injection. The membrane was equilibrated with the test solution for 30 to 45 min before force measurements were performed. The force measurements were conducted at five different locations, and at least 25 measurements were taken at each location. Data obtained from the retracting force curves were processed and converted to obtain the force versus surface-to-surface separation curves.

RESULTS AND DISCUSSION

Properties of the Nanoparticles Are Fine-Tuned for Membrane Functionalization. Silica nanoparticles were used because their surface chemistry can be readily fine-tuned, thereby facilitating the attainment of target hydrophilic properties and enabling control of the interaction with the

	Hydrodynamic radius using dynamic light scattering (nm)*		Electrophoretic mobility (μm·cm $V^{-1}s^{-1}$)
	Deionized water	Salt solution	Unadjusted pH
Bare silica	6.98 ± 0.11	8.15 ± 0.15	
-$N(CH_3)_3^+$	8.02 ± 0.16	11.55 ± 0.25	2.48 ± 0.09
-NH_2/NH_3^+	18.99 ± 0.35	20.52 ± 0.45	2.30 ± 0.19

*No aggregation observed within 45 minutes

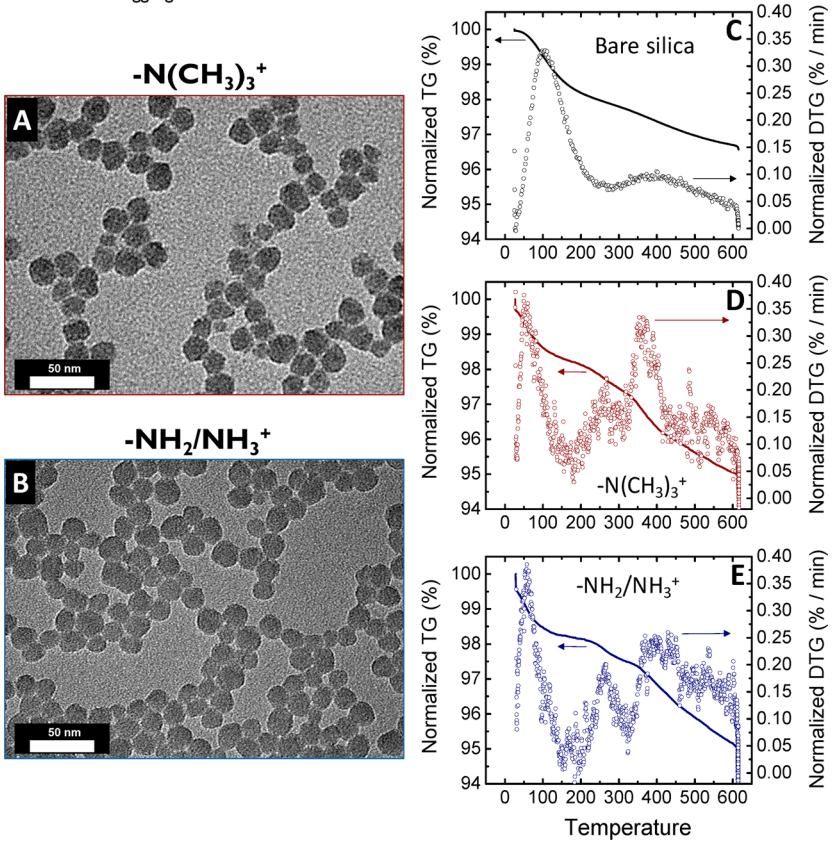

Figure 1. Size, electrophoretic mobility, and thermogravimetric analysis of the functionalized silica nanoparticles. The measured size and electrophoretic mobility of the nanoparticles in DI water and in an electrolyte solution representative of a typical wastewater effluent (0.45 mM KH_2PO_4, 9.20 mM NaCl, 0.61 mM $MgSO_4$, 0.5 mM $NaHCO_3$, 0.5 mM $CaCl_2$, and 0.935 mM NH_4Cl) are presented in the table. Panels A and B show TEM images of silica nanoparticles silanized with $-N(CH_3)_3^+$-terminated chains and $-NH_2$-terminated chains, respectively. The plots on the right present TGA data for the (C) bare silica nanoparticles as well as for the (D, E) functionalized nanoparticles. The thermogravimetric plot (line) refers to the left axis and the differential thermogravimetric plot (hollow circles) refers to the right axis. Both data sets were normalized by the initial sample mass.

membrane surface. Two different ligands were employed to functionalize the nanoparticle surface. Nanoparticles treated with *N*-trimethoxysilylpropyl-*N*,*N*,*N*-trimethylammonium chloride carry quaternary ammonium groups and are hereafter designated as $-N(CH_3)_3^+$ nanoparticles. The second treatment using (3-aminopropyl)trimethoxysilane produced nanoparticles with amine surface functionalities that are henceforth referred to as $-NH_2/NH_3^+$ nanoparticles.

Upon surface functionalization, the presence of ammonium or amine groups rendered the functionalized nanoparticles positively charged, as confirmed by measurements of their electrophoretic mobility (Figure 1). The charge of $-N(CH_3)_3^+$ nanoparticles is not significantly affected by solution pH, while the charging behavior of the $-NH_2/NH_3^+$ nanoparticles is dependent on solution pH through protonation/deprotonation.

The starting bare silica nanoparticles had a hydrodynamic radius of ∼7 nm, as observed by DLS measurements. The measured radius in DI water increased to ∼8 and ∼19 nm for the $-N(CH_3)_3^+$ and $-NH_2/NH_3^+$ functionalizations, respectively (Figure 1, table). While the small increase in diameter for the quarternary ammonium-functionalized nanoparticles is attributed to the presence of a hydration layer bound to the hydrophilic surface ligands, the increase in the size of the amine nanoparticles was likely due to slight aggregation. TEM imaging confirmed that the size of both types of functionalized nanoparticles was comparable to that of the bare silica nanoparticles (not shown). This observation substantiates our hypothesis that the $-NH_2/NH_3^+$ nanoparticles undergo aggregation in aqueous solution. No change in diameter was observed by DLS within 45 min of measurement for both functionalized nanoparticle types, suggesting that aggregation occurred immediately upon dispersion of the particle in solution. Overall, the positively charged surface groups increased the electrostatic repulsion between functionalized nanoparticles, thwarting their aggregation in aqueous solution.

In the presence of electrolytes in solution, DLS data demonstrated an increase in hydrodynamic size for all nanoparticles (Figure). This phenomenon can be due to

dx.doi.org/10.1021/am301532g | ACS Appl. Mater. Interfaces 2012, 4, 5044−5053

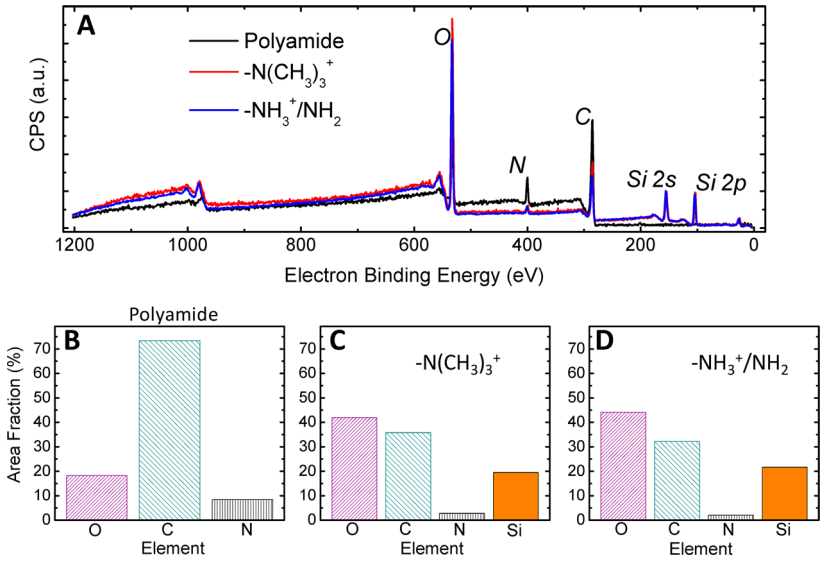

Figure 2. XPS analysis of the surface of the membranes. (A) XPS survey scan of control polyamide membranes (black), and of membranes functionalized with silica nanoparticles silanized with $-N(CH_3)_3^+$-terminated chains (red) and $-NH_2$-terminated chains (blue), (B, C, D) fractions of oxygen (O, purple), carbon (C, green), nitrogen (N, black), and silica (Si, orange) relative to the sum of these elements present at the surface of the three different membranes. The elemental fraction was calculated using software CasaXPS from the scans shown in Panel A. The two functionalized membranes show the presence of a significant amount of silica at their surface.

slight aggregation and/or to the adsorption of highly hydrated multivalent counterions onto the charged and hydrophilic particle surface. This mechanism could further enhance the structuring of the water molecules at the solid/liquid interface, resulting in a larger measured hydrodynamic diameter by DLS.[41−43]

The presence of organic ligands on the surface of the functionalized nanoparticles was confirmed by TGA measurement (Figures 1C−E). TGA data showed the appearance and amplification of two thermal degradation peaks (~250 and ~400 °C) for the functionalized nanoparticles. These peaks may be associated with thermo-oxidation of the alkyl chains of the surface ligands and possibly volatilization of some of the excess coupling agents used during particle functionalization. The production of a larger amount of volatile degradation products translated into a smaller percentage of sample recovery at the end of the heating cycle, compared to the bare silica nanoparticles.

Nanoparticles Are Irreversibly Bound to the Membrane Surface after Functionalization. All polyamide membranes fabricated via interfacial polymerization of TMC and MPD inherently possess an outer layer of relatively high, negative fixed charges resulting from incomplete reaction and hydrolysis of the TMC acyl chlorides to carboxyls.[32,44] The surface density of carboxylic groups of the membranes used in this study was measured by TBO 19 ± 4 charges/nm^2 of planar area. The positively charged groups at the nanoparticle surface ensure durable adhesion to the membrane surface via strong interaction with the native polyamide moieties, thus securing the nanoparticles at this interface. Specifically, the membrane−particle tethering occurred here primarily via electrostatic attraction.[45] In addition, the functionalization with $-NH_2$/NH_3^+ nanoparticles was performed in the presence of crosslinking agents EDC and NHS to facilitate the formation of covalent amide bonds between the nanoparticle amine groups and the membrane carboxyls.[12] The functionalized membranes are hereafter designated as $-N(CH_3)_3^+$ or $-NH_2$/NH_3^+ membranes.

XPS data of the membrane surfaces evaluated before and after functionalization are presented in Figure 2. The energy peaks observed for the polyamide surface (black) are attributed to carbon, oxygen, and nitrogen (Figure 2A), among which carbon was the most abundant element (Figure 2B), consistent with the chemistry of the membrane active layer. The spectra related to the functionalized surfaces (blue and red) showed the appearance of energy peaks associated with silicon (Figure 2A), which confirm the presence of the silica-based nanoparticles at these surfaces. Because XPS analyzes only the superficial portion of the membrane, oxygen was observed to be the predominant element, followed by carbon and silicon (see Figures 2C and 2D), according to the composition of the functionalized silica nanomaterial. ATR-IR spectra showed the emergence of a shoulder and an increase in absorbance at ~1060−1100 cm^{-1} (see Figure S1 in the Supporting Information), which is attributed to the stretching mode of Si−O−Si bonds.[46] This observation further confirms the presence of silanized SiO_2 nanoparticles at the membrane surface.

Physicochemical Properties of the Membrane Surface. Figure 3 presents the pH-dependent zeta potential of the membrane surfaces before and after functionalization. The zeta potential was measured over the pH range of 4−9 for at least four separately cast and functionalized membrane samples. Knowledge of the membrane surface zeta potential and of the type and density of exposed charges is crucial, because these parameters greatly influence the membrane fouling behavior.[40,47]

The results with the control membranes were in accordance with the protonation behavior of polyamide functional groups. At very low pH, the unreacted amine groups of MPD are protonated while carboxylic groups are uncharged, resulting in an overall positive potential (Figure 3A). As the pH increased above the pK_a of the polyamide carboxyl groups,[48] these predominant acidic groups deprotonated, thus imparting a negative and largely constant zeta potential to the surface.

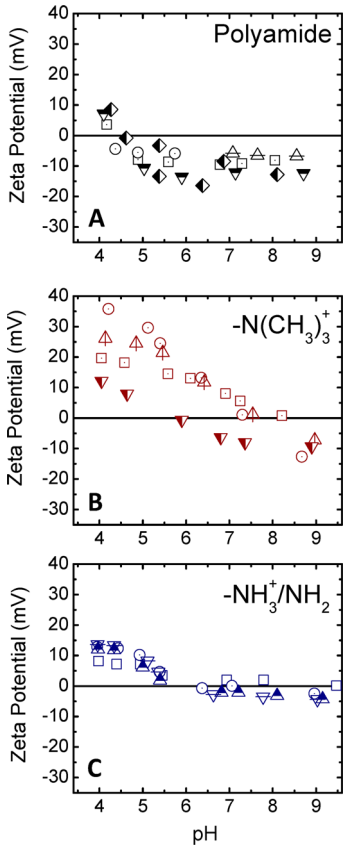

Figure 3. Zeta potential of the surface of the membranes as a function of solution pH. (A) Zeta potentials of polyamide control membranes, and (B, C) zeta potentials of membranes functionalized with silica nanoparticles silanized with (red) $-N(CH_3)_3^+$-terminated chains and (blue) $-NH_2$-terminated chains, respectively. Zeta potential values were measured and calculated for at least four separately cast and functionalized samples for each membrane type, across a pH range from ~4 to 9. The data related to different samples were placed in the same plot and represented by different symbols. Measurements were taken at room temperature (23 °C), in solution of 1 mM KCl, and by adjusting the pH with appropriate amounts of HCl or KOH.

The zeta potential behavior of the functionalized membranes was consistent with the functionalities present at both the nanoparticle and the membrane surface. The $-N(CH_3)_3^+$ nanoparticles are positively charged at all pH values and interact with the membrane carboxylic moieties via electrostatic attraction. Therefore, the zeta potential of the membranes was highly positive at low pH, where carboxyl groups are uncharged, and became progressively more negative as the carboxylic groups deprotonated (Figure 3B). The overall zeta potential was close to zero near the pH range of 7–8, which is the characteristic pH of natural waters and wastewater effluents in membrane separation processes.

Nanoparticles functionalized with $-NH_2/NH_3^+$ ligands are assumed to preferentially form amide bonds with the membrane carboxylic groups, thus effectively neutralizing many of the charges present on both reacting surfaces. As a result, the measured zeta potential values of the $-NH_2/NH_3^+$ membranes were of lower magnitude, compared to those of the $-N(CH_3)_3^+$ membranes and exhibited a wider near-zero potential region, between pH ~6 and pH ~8 (see Figure 3C). The zeta potential results provide indirect evidence for the presence of nanoparticles at the surface of the functionalized membranes and for the type of particle–membrane interaction.

The membrane surface morphology before and after functionalization was analyzed by SEM and atomic force microscopy (AFM) (see Figure 4). The representative topographic image (Figure 4G) and SEM surface micrographs (Figures 4A and 4B) of a control polyamide membrane showed a uniform ridge-and-valley morphology, which is typical of polyamide thin films formed by interfacial condensation.[1,4] The characteristic surface roughness parameters of the membranes were measured by tapping-mode AFM. The untreated polyamide surfaces had a RMS of 129 ± 40 nm, an average roughness (R_a) of 102 ± 39 nm, a maximum roughness (R_{max}) of 850 ± 30 nm, and a surface area difference (SAD) of 23% ± 10% (see Figure 4H). These values are comparable to those reported for similar materials.[49]

The high magnification SEM micrographs in Figures 4B, 4D, and 4F, imaged at the surface of the membranes after functionalization, showed that the ridge-and-valley features of the functionalized surfaces were overlaid by a layer of nanoparticles. The nanoparticle size correlates well with the radius measured by DLS experiments for each respective type of surface functionality. The low-magnification SEM micrographs presented in Figures 4A, 4C, and 4E suggest that the overall morphology of the membrane surface was not significantly affected after functionalization, as the ridge-and-valley features were visible and comparable to those observed for the control polyamide surface. This observation suggests that the nanoparticle coating consisted of a mono- or multilayer, with a total thickness small relative to the roughness of the membrane active layer.

The surface roughness measurements of functionalized membranes (Figure 4H) indicated a reduction in surface roughness that was due to the presence of nanoparticles, although it was not sufficient to alter the overall surface morphology, consistent with SEM analysis. The nanoparticles are likely to deposit preferentially within the valley-like regions of the polyamide surface, thus flattening the overall surface. This flattening was more pronounced for the relatively larger $-NH_2/NH_3^+$ nanoparticles, which produced a more significant effect in decreasing the membrane SAD (see Figure 4H and Table 1).

Nanoparticles Render the Membrane Highly Hydrophilic. Figure 5 presents the average contact angles of DI water at the surface of control (polyamide) and functionalized membranes before (solid bar) and after (hollow bars) they were subjected to chemical and physical stresses. The untreated polyamide membranes had a contact angle of 104° ± 16°, which was larger than what is typically observed for commercial polyamide membranes (see Figure 5, Table 1). For rough surfaces, such as those of our hand-cast samples, larger contact angles than expected from the chemistry of the material might result from air trapped between the solid surface rugosities and the liquid droplet.[50] The digital picture (Figure 5A) shows a representative profile of a water droplet on the hydrophobic polyamide surface. The presence of nanoparticles on the surface functionalized membranes had a dramatic effect on the conformation of water droplets at the solid/liquid interface, yielding contact angles of ~10° for the $-N(CH_3)_3^+$ membranes and ~20° for the $-NH_2/NH_3^+$ membranes (see Table 1), only in part attributable to the decrease in roughness measured on the functionalized surfaces (Figure 4). Representative pictures

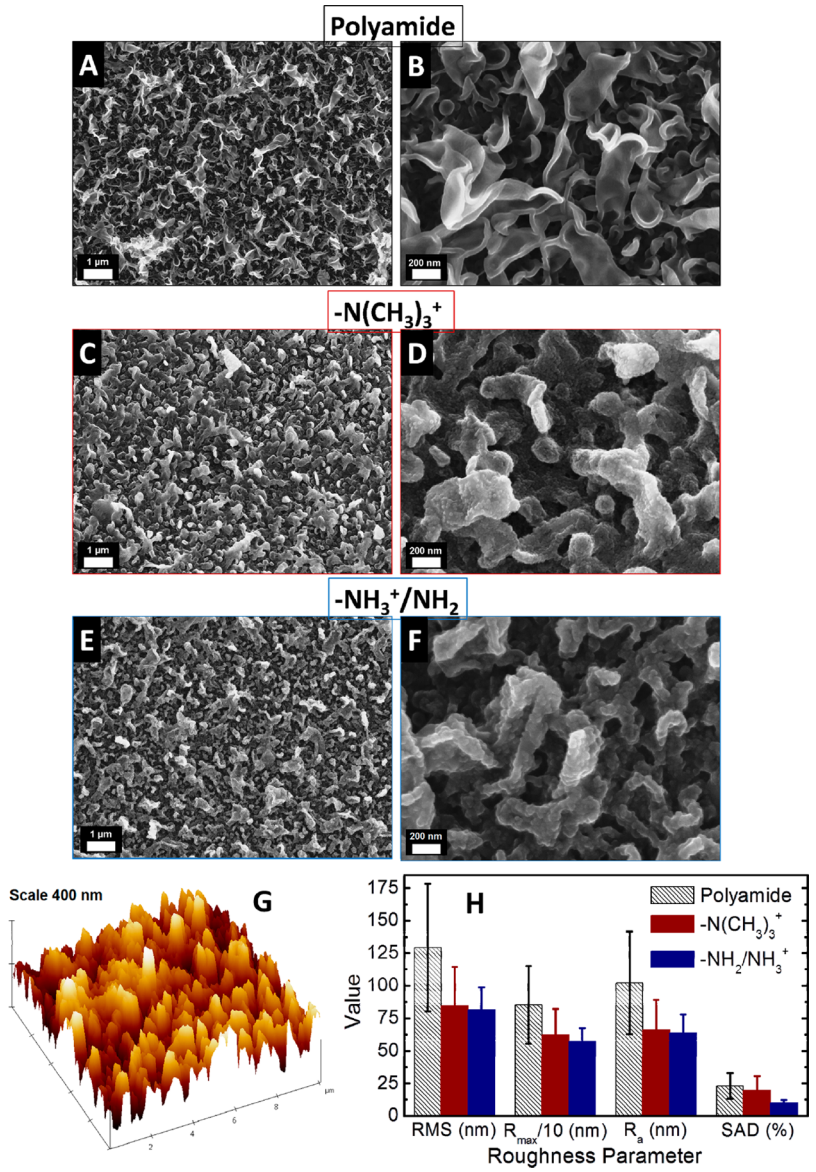

Figure 4. Surface morphology and roughness of the membranes from SEM and AFM analyses. Surface SEM micrographs of (A, B) polyamide control membranes, (C, D) membranes functionalized with silica nanoparticles silanized with $-N(CH_3)_3^+$-terminated chains, and (E, F) membranes functionalized with silica nanoparticles silanized with $-NH_2$-terminated chains. Panels A, C, and E are low-magnification micrographs, while panels B, D, and F are higher-magnification surface images. (G) Representative AFM image of a control polyamide membrane. (H) Roughness parameters measured by AFM tapping mode analysis. Here, RMS is the root mean square of roughness, $R_{max}/10$ is the maximum roughness divided by a factor of 10, R_a is the average roughness, and SAD is a percentage surface area difference. Black, red, and blue bars refer to polyamide membranes, and membranes functionalized with $-N(CH_3)_3^+$- and $-NH_2$-coated nanoparticles, respectively. Roughness values are the average of measurements taken from a total of 12 random spots on three separately cast and functionalized sample surfaces.

Table 1. Summary of the Contact Angle and Surface Energy Data of the Different Membranes Analyzed in This Study[a]

membrane	θ_{wat}	θ_{gly}	θ_{diod}	SAD (%)	γ^{LW}	γ^+	γ^-	γ^{AB}	γ^{TOT}	$-\Delta G_{ML}$	ΔG_{MLM} (TOT)
polyamide	105	76.5	27.2	23.0	37.7	0.06	0.03	0.09	37.8	57.9	−97.9
$-N(CH_3)_3^+$	<10	17.6	18.3	19.3	41.0	1.10	38.3	13.0	54.0	133	+12.3
$-NH_3^+/NH_2$	19.9	23.7	25.7	9.9	42.1	1.2	39.4	13.9	55.9	135	+12.7

[a]Average contact angles of the water, glycerol, and diiodomethane are reported (in degrees), along with the different components of the surface energy of the membrane surface, expressed in units of mJ/m^2.

of water droplet profiles for the two functionalized surfaces are presented on the right-hand side of Figure 5B.

Contact angle measurements were also used as a proxy to appraise the reversibility of the interaction between nanoparticles and membrane surfaces. Chemical or physical stresses considerably harsher than typical operational conditions were applied to the functionalized membranes and the conformation of water droplets was then re-evaluated. The contact angles did not change significantly, compared to membranes analyzed immediately after modification (see Figures 5A and 5B),

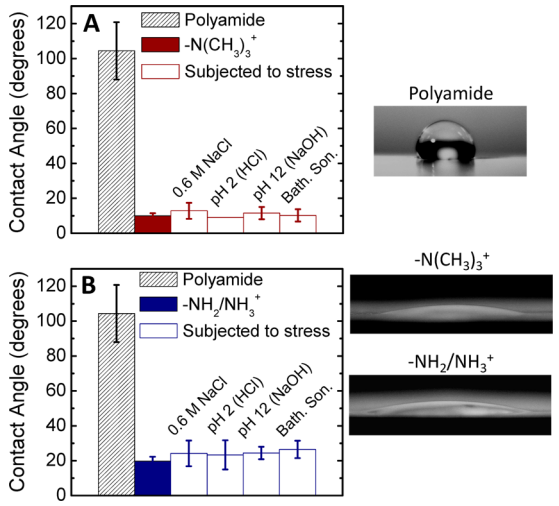

Figure 5. Contact angles of DI water on the surface of the membranes for (A) membranes functionalized with silica nanoparticles silanized with $-N(CH_3)_3^+$-terminated chains (red), and (B) membranes functionalized with silica nanoparticles silanized with $-NH_2$-terminated chains (blue). The contact angle of DI water on control polyamide membranes is shown in both plots as a patterned black bar. The plots show values of the membranes as functionalized (solid bars), and after the surface was subjected to stress (hollow bars), as briefly labeled in the graphs on each bar and as described in the discussion. Values are averages of at least 8 random spots from each sample. Measurements were carried out at room temperature (23 °C), without addition of ionic strength, and at unadjusted pH. When contact angles were too low to be accurately measured, a value of 10° was assumed for the calculations. Representative pictures of DI water droplets are included on the right-hand side for illustration purposes.

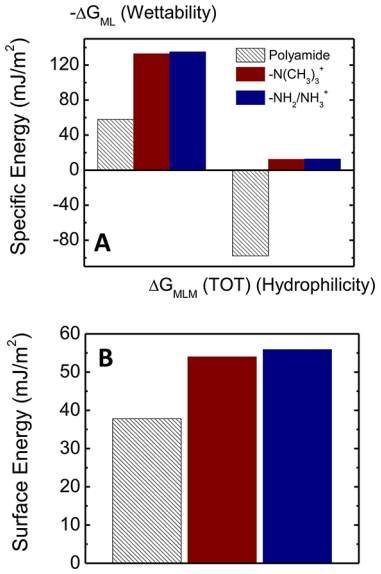

Figure 6. Wettability, hydrophilicity, and surface energy of the surface of the membranes. (A) Wettability with DI water ($-\Delta G_{ML}$) and hydrophilicity (ΔG_{MLM}(TOT)) and (B) calculated values of surface energy (γ^{TOT}). Data for polyamide control membranes are presented as black patterned bars. Values for membranes functionalized with silica nanoparticles silanized with $-N(CH_3)_3^+$-terminated chains or with $-NH_2$-terminated chains are shown as red and blue bars, respectively. The surface energy parameters were calculated from average contact angles measured with DI water, glycerol, and diiodomethane at room temperature (23 °C), without addition of ionic strength, and at unadjusted pH. At least 25 contact angles on at least three separately cast and functionalized samples were measured for each liquid and for each membrane type.

suggesting that the nanoparticle–membrane bonds were sufficiently strong to render the surface functionalization irreversible. XPS and SEM analyses were also performed subsequent to the stress protocol and showed no significant difference, compared to the results obtained on the functionalized membranes not subjected to stresses (see Figure S2 in the Supporting Information). The confirmed strength of the nanoparticle–membrane interaction suggests minimal detachment of the nanoparticles from the surface during typical membrane operational conditions, thus ensuring long-term functionalization.

The surface tensions and interfacial free energies of the membranes were calculated from contact angle measurements with two polar liquids, water and glycerol, and an apolar liquid, diiodomethane (Table 1). The polyamide control membrane had a relatively low surface energy (γ^{TOT} = 37.8 mJ/m^2), almost exclusively resulting from van der Waals forces. As a result, the polyamide surface was found to be relatively wetting ($-\Delta G_{ML}$ = 57.9 mJ/m^2), but hydrophobic (ΔG_{MLM} = −97.9 mJ/m^2) when immersed in DI water (see Figure 6). These results are consistent with data obtained from other polyamide membranes.[38,51]

The surface properties of the membranes changed dramatically after functionalization with superhydrophilic nanoparticles. Both the Lifshitz–van der Waals and the acid–base components of surface tensions increased. In particular, the electron donor parameter was responsible for the nearly monopolar functionality of the surface (Table 1), consistent with the properties of the ligands coating the nanoparticle surface.[52,53] The high density of electron donor sites at the surface of the functionalized membranes promotes hydrogen bonding interactions with water molecules.[54] This, in turn, resulted in a significant increase in calculated membrane wettability and a conversion of the surface interfacial free energy of cohesion to positive values, i.e., hydrophilic properties (Figure 6A). The values of hydrophilicity estimated for our functionalized membranes are the highest reported so far in the literature for similar materials. The high interfacial free energy was accompanied by a relatively large value of surface energy (Figure 6B). The strong hydration layer of the near superhydrophilic surface resists the adsorption of molecules and particles to the membrane surface, thus increasing its antifouling resistance.[17]

Hydrophilic Membranes Have Lower Interaction Forces with Organic Foulants. The rationale for creating highly hydrophilic membranes for water separation technologies is to impart fouling resistance. By maximizing the interfacial acid–base forces between surfaces and the adherent water, we form a layer of tightly bonded water molecules that act as a short-range barrier against the adhesion of foulants.[20] Atomic force microscopy (AFM) has been applied in membrane fouling/cleaning research to quantify intermolecular forces when foulants approach the investigated surface within the contact limit.[6,20,40,55,56] In this study, we investigated the interaction forces between model foulants adsorbed on a colloidal probe (namely, alginate and BSA) and our membranes (see Figure 7). Representative adhesion (pull-off) curves obtained during the retraction of the fouled tip from the membrane surface are presented. We also report the average, minimum, and maximum values of adhesion forces calculated

dx.doi.org/10.1021/am301532g | ACS Appl. Mater. Interfaces 2012, 4, 5044–5053

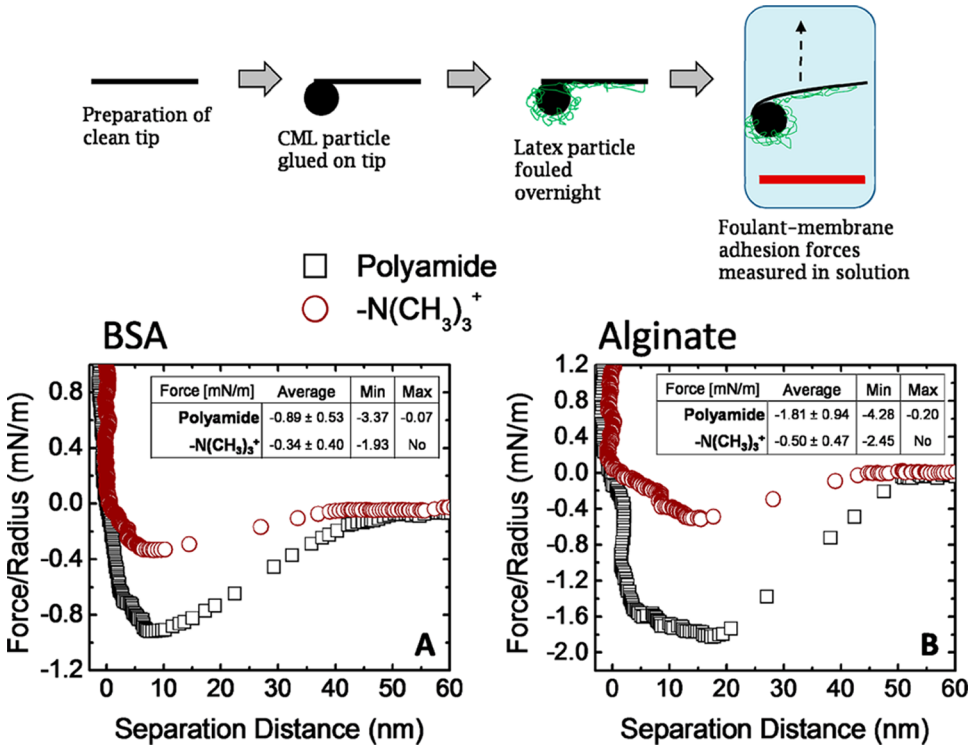

Figure 7. Representative atomic force microscopy (AFM) retraction curves for foulant–membrane interaction using (A) a BSA-fouled tip, and (B) an alginate-fouled tip. Data for the control polyamide and for membranes functionalized with $-N(CH_3)_3^+$-terminated nanoparticles are shown as black squares and red circles, respectively. The average, minimum, and maximum values of the minimum energy wells measured for 125 separate retracting curves are reported for each foulant. The "No" label represents measurements where no adhesion force was observed. The test solution for the measurements is synthetic wastewater as described in the experimental section. Measurements were carried out at room temperature (23 °C).

from a statistically significant number of retracting force–distance curves analyzed in five randomly selected spots on each membrane sample.

AFM results showed that the attractive energy well between model foulants and the control polyamide membranes was deeper than that observed using functionalized, hydrophilic membranes (see Figures 7A and 7B). The resulting distribution of foulant–membrane intermolecular forces was also statistically more negative (i.e., more attractive) for the control polyamide membranes (see Figure S3 in the Supporting Information). Several force–distance curves measured on $-N(CH_3)_3^+$ membranes did not show an attractive energy well but only repulsive forces, indicating no foulant adhesion to the membrane, because of a barrier to adhesion.[57] This behavior was not observed for control polyamide membranes on which all AFM foulant probe engagements resulted in an attractive force, often exceeding −3 mN/m for both foulant molecules. These results are consistent with previous observations showing lower attractive forces on hydrophilic surfaces,[20] and they indicate the attainment of highly hydrophilic surfaces with potentially lower fouling propensity. The antifouling behavior and antifouling mechanisms of our highly hydrophilic membranes were further confirmed in cross-flow experiments in forward-osmosis and reverse-osmosis operation modes, using feed solutions of BSA or alginate, as described in our related publication.[30]

CONCLUSION

We fabricated forward osmosis membranes with near superhydrophilic surface properties that could significantly reduce fouling. The surface of silica nanoparticles was functionalized with superhydrophilic ligands possessing quaternary ammonium or amine moieties. A simple dip-coating technique was utilized to irreversibly bind the nanoparticles to the native carboxylic groups of polyamide forward-osmosis membranes. The functionalization produced a uniform layer of nanoparticles on the polyamide film rendering the membrane surface highly wettable and hydrophilic. The post-fabrication route to functionalization ensures that the productivity and the rejection performance of the membranes are maintained. Using atomic force microscopy (AFM), we measured significantly lower adhesion forces between model organic foulants and the hydrophilic surfaces, compared to unmodified polyamide membranes. These observations are significant because lower foulant-membrane adhesion has been shown to correlate well with increased membrane fouling resistance.

ASSOCIATED CONTENT

Supporting Information

ATR-IR analysis of the membrane surfaces confirming presence of silica nanoparticles after membrane functionalization (Figure S1); XPS and SEM analyses of the membrane surface performed after subjecting the membrane surface to stress, confirming the irreversibility of surface functionalization (Figure S2); statistics of foulant-membrane interaction forces measured by AFM (Figure S3); summary of forward osmosis membrane performance testing conditions and results (Table S4). This material is available free of charge via the Internet at http://pubs.acs.org.

AUTHOR INFORMATION

Corresponding Author

*Tel. +1 (203) 432-2789. Fax: +1 (203) 432-4387. E-mail: menachem.elimelech@yale.edu.

Notes

The authors declare no competing financial interest.

ACKNOWLEDGMENTS

This publication is based on work supported by Award No. KUS-C1-018-02, made by King Abdullah University of Science and Technology (KAUST). We also acknowledge the NWRI-AMTA Fellowship for Membrane Technology, awarded to A.T.

REFERENCES

(1) Elimelech, M.; Phillip, W. A. *Science* **2011**, *333* (6043), 712.
(2) McGinnis, R. L.; Elimelech, M. *Environ. Sci. Technol.* **2008**, *42* (23), 8625.
(3) McGinnis, R. L.; Elimelech, M. *Desalination* **2007**, *207* (1−3), 370.
(4) Petersen, R. J. *J. Membr. Sci.* **1993**, *83* (1), 81.
(5) Geise, G. M.; Park, H. B.; Sagle, A. C.; Freeman, B. D.; McGrath, J. E. *J. Membr. Sci.* **2011**, *369* (1−2), 130.
(6) Ang, W. S.; Tiraferri, A.; Chen, K. L.; Elimelech, M. *J. Membr. Sci.* **2011**, *376* (1−2), 196.
(7) Mi, B. X.; Elimelech, M. *J. Membr. Sci.* **2010**, *348* (1−2), 337.
(8) Rana, D.; Matsuura, T. *Chem. Rev.* **2010**, *110* (4), 2448.
(9) Kang, G. D.; Cao, Y. M. *Water Res.* **2012**, *46* (3), 584.
(10) Kim, S. H.; Kwak, S. Y.; Sohn, B. H.; Park, T. H. *J. Membr. Sci.* **2003**, *211* (1), 157.
(11) Mo, J.; Son, S. H.; Jegal, J.; Kim, J.; Lee, Y. H. *J. Appl. Polym. Sci.* **2007**, *105* (3), 1267.
(12) Tiraferri, A.; Vecitis, C. D.; Elimelech, M. *ACS Appl. Mater. Interfaces* **2011**, *3* (8), 2869.
(13) Herzberg, M.; Elimelech, M. *J. Membr. Sci.* **2007**, *295* (1−2), 11.
(14) De Kwaadsteniet, M.; Botes, M.; Cloete, T. E. *Nano* **2011**, *6* (5), 395.
(15) Upadhyayula, V. K. K.; Gadhamshetty, V. *Biotechnol. Adv.* **2010**, *28* (6), 802.
(16) Stanley, M. S.; Callow, M. E.; Callow, J. A. *Planta* **1999**, *210* (1), 61.
(17) Callow, J. A.; Callow, M. E. *Nat. Commun.* **2011**, 2.
(18) Herzberg, M.; Kang, S.; Elimelech, M. *Environ. Sci. Technol.* **2009**, *43* (12), 4393.
(19) Shannon, M. A.; Bohn, P. W.; Elimelech, M.; Georgiadis, J. G.; Marinas, B. J.; Mayes, A. M. *Nature* **2008**, *452* (7185), 301.
(20) Morra, M. *J. Biomater. Sci., Polym. Ed.* **2000**, *11* (6), 547.
(21) Finlay, J. A.; Callow, M. E.; Ista, L. K.; Lopez, G. P.; Callow, J. A. *Integr. Comput. Biol.* **2002**, *42* (6), 1116.
(22) Wavhal, D. S.; Fisher, E. R. *Langmuir* **2003**, *19* (1), 79.
(23) Gudipati, C. S.; Finlay, J. A.; Callow, J. A.; Callow, M. E.; Wooley, K. L. *Langmuir* **2005**, *21* (7), 3044.
(24) Ostuni, E.; Chapman, R. G.; Holmlin, R. E.; Takayama, S.; Whitesides, G. M. *Langmuir* **2001**, *17* (18), 5605.
(25) Brant, J. A.; Childress, A. E. *J. Membr. Sci.* **2004**, *241* (2), 235.
(26) Ang, W. S.; Lee, S. Y.; Elimelech, M. *J. Membr. Sci.* **2006**, *272* (1−2), 198.
(27) Tiraferri, A.; Yip, N. Y.; Phillip, W. A.; Schiffman, J. D.; Elimelech, M. *J. Membr. Sci.* **2011**, *367* (1−2), 340.
(28) Yip, N. Y.; Tiraferri, A.; Phillip, W. A.; Schiffman, J. D.; Elimelech, M. *Environ. Sci. Technol.* **2010**, *44* (10), 3812.
(29) Yip, N. Y.; Tiraferri, A.; Phillip, W. A.; Schiffrnan, J. D.; Hoover, L. A.; Kim, Y. C.; Elimelech, M. *Environ. Sci. Technol.* **2011**, *45* (10), 4360.
(30) Tiraferri, A.; Kang, Y.; Giannelis, E.; Elimelech, M. Submitted to *Environ. Sci. Technol.*, **2012**.
(31) Tiraferri, A.; Chen, K. L.; Sethi, R.; Elimelech, M. *J. Colloid Interface Sci.* **2008**, *324* (1−2), 71.
(32) Tiraferri, A.; Elimelech, M. *J. Membr. Sci.* **2012**, *389*, 499.
(33) Staros, J. V.; Wright, R. W.; Swingle, D. M. *Anal. Biochem.* **1986**, *156* (1), 220.
(34) Ghosh, A. K.; Jeong, B. H.; Huang, X. F.; Hoek, E. M. V. *J. Membr. Sci.* **2008**, *311* (1−2), 34.
(35) Wenzel, R. N. *J. Phys. Colloid Chem.* **1949**, *53* (9), 1466.
(36) Van Oss, C. J. *J. Adhes. Sci. Technol.* **2002**, *16* (6), 669.
(37) van Oss, C. J.; Wu, W.; Docoslis, A.; Giese, R. F. *Colloid Surf. B* **2001**, *20* (1), 87.
(38) Hurwitz, G.; Guillen, G. R.; Hoek, E. M. V. *J. Membr. Sci.* **2010**, *349* (1−2), 349.
(39) Walker, S. L.; Bhattacharjee, S.; Hoek, E. M. V.; Elimelech, M. *Langmuir* **2002**, *18* (6), 2193.
(40) Li, Q. L.; Elimelech, M. *Environ. Sci. Technol.* **2004**, *38* (17), 4683.
(41) Butkus, M. A.; Grasso, D. *J. Colloid Interface Sci.* **1998**, *200* (1), 172.
(42) Derjaguin, B. V.; Churaev, N. V. *Langmuir* **1987**, *3* (5), 607.
(43) Leberman, R.; Soper, A. K. *Nature* **1995**, *378* (6555), 364.
(44) Freger, V. *Langmuir* **2003**, *19* (11), 4791.
(45) Fang, J.; Kelarakis, A.; Estevez, L.; Wang, Y.; Rodriguez, R.; Giannelis, E. P. *J. Mater. Chem.* **2010**, *20* (9), 1651.
(46) Mawhinney, D. B.; Glass, J. A.; Yates, J. T. *J. Phys. Chem. B* **1997**, *101* (7), 1202.
(47) Wiesner, M. R.; Chellam, S. *Environ. Sci. Technol.* **1999**, *33* (17), 360A.
(48) Vrijenhoek, E. M.; Hong, S.; Elimelech, M. *J. Membr. Sci.* **2001**, *188* (1), 115.
(49) Tang, C. Y. Y.; Kwon, Y. N.; Leckie, J. O. *Desalination* **2009**, *242* (1−3), 168.
(50) van Oss, C. J.; Giese, R. F.; Docoslis, A. *J. Dispersion Sci. Technol.* **2005**, *26* (5), 585.
(51) Brant, J. A.; Childress, A. E. *J. Membr. Sci.* **2002**, *203* (1−2), 257.
(52) Chatterjee, A.; Balaji, T.; Matsunaga, H.; Mizukami, F. *J. Mol. Graph. Modell.* **2006**, *25* (2), 208.
(53) He, T.; Ding, H. J.; Peor, N.; Lu, M.; Corley, D. A.; Chen, B.; Ofir, Y.; Gao, Y. L.; Yitzchaik, S.; Tour, J. M. *J. Am. Chem. Soc.* **2008**, *130* (5), 1699.
(54) Vanoss, C. J.; Chaudhury, M. K.; Good, R. J. *Adv. Colloid Interface Sci.* **1987**, *28* (1), 35.
(55) Tang, C. Y.; Kwon, Y. N.; Leckie, J. O. *J. Membr. Sci.* **2009**, *326* (2), 526.
(56) Lee, S.; Ang, W. S.; Elimelech, M. *Desalination* **2006**, *187* (1−3), 313.
(57) Adout, A.; Kang, S.; Asatekin, A.; Mayes, A. M.; Elimelech, M. *Environ. Sci. Technol.* **2010**, *44* (7), 2406.